Available online at www.sciencedirect.com
SCIENCE DIRECT®
Bioorganic & Medicinal Chemistry 12 (2004) 6119–6135
Bioorganic & Medicinal Chemistry

Fluorescent ε-ATP analogues for probing physicochemical properties of proteins. Synthesis, biochemical evaluation, and sensitivity to properties of the medium

Einat Sharon,[a] Gregor Zündorf,[b] Sébastien A. Lévesque,[c] Adrien R. Beaudoin,[c] Georg Reiser[b] and Bilha Fischer[a,*]

[a]*Department of Chemistry, Gonda-Goldschmied Medical Research Center, Bar-Ilan University, Ramat-Gan 52900, Israel*
[b]*Institute for Neurobiochemistry, Faculty of Medicine, Otto von Guericke University, Leipziger Str. 44, D-39120 Magdeburg, Germany*
[c]*Department of Biology, Faculty of Sciences, University of Sherbrooke, Canada J1K 2R1*

Received 12 March 2004; accepted 6 September 2004
Available online 30 September 2004

Abstract—Despite the significance of the elucidation of proteins' physicochemical parameters to understand various molecular phenomena, direct methods for measuring these parameters are not readily available. Here, we propose the use of 8-[*p*-amino-Ph]-ε-ATP, **3b**, as a fluorescent probe for the elucidation of physicochemical parameters of binding sites in certain proteins. We synthesized novel fluorescent nucleotide analogues based on an extension of the ε-ATP scaffold. These analogues bear a primary or tertiary *p*-amino-phenyl moiety on the etheno-bridge. We explored the recognition of the fluorescent analogues by the target proteins: $P2Y_1$-receptor ($P2Y_1$-R) and NTPDase1. Based on the high affinity to the $P2Y_1$-R (EC_{50} 100 nM), **3b** proved a suitable probe for the investigation of this receptor. Next, we elucidated the dependencies of the absorption and emission spectra of **3b** on environmental parameters, for establishing correlation equations. These equations will help determine the properties of the ATP-binding site from the spectral data of the protein-bound **3b**. For this purpose, the sensitivity of the probe to acidity, dielectricity, H-bonding, viscosity, and to correlation between these parameters was determined. Thus, the pH-dependence of **3b** emission intensity is bell shaped. At pH 2.8 the quantum yield (ϕ) is enhanced 150-fold, as compared to neutral pH. The basic nitrogen atoms of **3b** were assigned and pK_a values were determined. A linear relationship was found between $\log\phi$ and log viscosity, however, emission maxima (λ_{max}) remained constant. A linear relationship was found between both ϕ and λ_{max} and dielectricity, as measured in protic or aprotic solvents of comparable viscosity. pK_a-like values were measured in acid-titrated alcohols with varying dielectricity but comparable viscosity, or with varying viscosity but comparable dielectricity. An inverse relationship and a linear relationship were found between the pK_a values of **3b** and the medium dielectricity and viscosity, respectively. These correlations help the calibration of properties of a protein ATP-binding site.

1. Introduction

A binding pocket within a protein can be regarded as a medium affecting the solvation of the protein-bound molecule. Unlike solvents, this medium is not homogeneous, yet, it provides the bound molecule with an effective polarity, viscosity, and acidity. Warshel suggested that enzymes can be considered as 'super-solvents' that stabilize unstable intermediates. For instance, proteins stabilize ionic transition states more effectively than aqueous solutions.[1] Stabilization is due to the unique physicochemical properties of the binding pocket, including both general and specific (e.g., H-bonds, protonation) interactions. Despite the significance of these physicochemical parameters for the understanding of various molecular phenomena, such as molecular recognition and enzymatic mechanisms, and for calculating molecular models of proteins, direct methods for measuring these parameters in proteins binding pockets are not readily available.

Nevertheless, indirect methods have been proposed for the measurement of polarity,[2] acidity,[2–4] and viscosity[5,6] of proteins.

Keywords: Fluorescence; ε-ATP; Proteins; Viscosity; Dielectricity; Acidity.
* Corresponding author. Tel.: +972 3 5318303; fax: +972 3 5351250; e-mail: bfischer@mail.biu.ac.il

0968-0896/$ - see front matter © 2004 Elsevier Ltd. All rights reserved.
doi:10.1016/j.bmc.2004.09.011

The inherent limitations in the measurement of physicochemical properties of a protein binding site, prompted us to propose an indirect method for probing these properties in ATP-binding proteins. As a continuation of our work in the field of molecular recognition of adenine nucleotides,[7] we targeted the investigation of a nucleotide receptor, $P2Y_1$-R, and NTPDase1 that are both responsible for ATP signaling.

The method proposed here involves the use of a new fluorescent probe based on the well-known etheno-(ε)-ATP, **1a**, scaffold.[8] In an earlier study, we reported the unique fluorescent characteristics of 8-(*p*-amino-phenyl)-3-β-D-ribofuranosylimidazo[2,1-i]purine-5′-monophosphate, **3a**.[9] These findings encouraged us to further explore the possible use of related analogues as fluorescent probes.

Here, we report on the synthesis and spectral properties of a series of ε-adenine nucleotide derivatives **3**–**5**. These analogues bear *p*-amino-phenyl substituents on the etheno-bridge at the C8-position. In addition, we report on the biochemical relevance of analogue **3b** for the investigation of our target proteins, $P2Y_1$-receptor, and NTPDase1. We describe the sensitivity of probe **3b** to various environmental physicochemical parameters. Specifically, we report on the dependence of emission spectra of probe **3b** on pH, viscosity, dielectricity, and H-bonds. Furthermore, we describe the dependence of the spectra of **3b** on correlations between dielectricity/H-bonding and acidity, and between viscosity/H-bonding and acidity.

The spectral results described here will be used for establishing correlation equations. These equations will help interpret the spectral properties of the protein-bound probe in terms of the average environment surrounding the fluorophore. This application will be published in due course.

2. Results

2.1. Synthesis of fluorescent probes 2–5

Since ATP has poor fluorescence properties,[10] we chose fluorophores that display improved spectral properties. Furthermore, because proteins absorb light near 280 nm, and fluorescence emission maxima range from 320 to 350 nm, we chose probes that are excited and emit outside the wavelength range of proteins.

The design of the new fluorescent nucleotide probes is based on the ε-ATP scaffold, **1a**.[8] The C8-aryl substitution on this scaffold produced fluorescent and environment-responsive probes **3**–**5**, Scheme 1.[9]

Previously, we reported the synthesis of aryl-substituted ε-adenine nucleotides **2a** and **3a**.[9] The synthesis of **2a** harnessed the Kornblum oxidation reaction[11,12] to assist with the formation of the substituted etheno-bridge.

In a typical procedure, AMP free acid, or ATP tetrakis-(Bu_4N^+) salt, was dissolved in DMSO together with excess of 2-Br-(*p*-NO_2)-acetophenone, and pH 4.5 was maintained. After 12 h at room temperature products **2a** or **2b** were isolated as single regioisomers in ca. 70% yield.[13] Regiochemistry was assigned by NOESY spectrum.

Since substituents that donate electrons to the π system enhance absorption of light and increase fluorescence, we prepared the corresponding 8-(*p*-amino-phenyl)-ε-adenine nucleotides, **3**–**5** from the *p*-nitrophenyl precursor **2**. Analogues **3a**,**b** were obtained in quantitative yields by catalytic hydrogenation of **2** over PtO_2.

Derivatives **4a**,**b** and **5a**,**b** were prepared in high yields in a one-pot reduction–alkylation of the *p*-nitro function. The nitro group was first reduced to a primary amine, followed by tandem Schiff-base formation, with formaldehyde or acetaldehyde, respectively, and reduction to the corresponding dimethyl and diethyl tertiary amine analogues (Scheme 2).[14]

2.2. Biochemical evaluation of probes 2–5

The investigation of the affinity of analogues **2**–**5** to the target proteins is a pre-requisite to their application as probes. Therefore, analogues **2**–**5** were evaluated either as ligands of a $P2Y_1$-receptor or substrates/inhibitors of NTPDase1.

2.3. Evaluation of analogues 3b–5b as $P2Y_1$-R agonists

To examine the efficacy of analogues **3b**–**5b** in a functional assay, we tested them by the agonist-induced Ca^{2+} release in HEK 293 cells stably transfected with rat brain $P2Y_1$-receptor (Fig. 1).[15] Those $P2Y_1$-R-transfected cells were shown to be suitable for pharmacological characterization.[16] Analogue **3b**, with EC_{50} of 1×10^{-7} M, was found to be almost equipotent with ATP, EC_{50} of 2×10^{-7} M. However, dialkyl substitution on the *p*-amino function of **3b**, as in analogues **4b** and **5b**, reduced the ligand's potency. This resulted in EC_{50} value of 5×10^{-7} M for **4b** and a clear reduction by one order of magnitude for **5b**, EC_{50} of 1.5×10^{-6} M.

2.4. Evaluation of analogues 2b–5b interaction with NTPDase1 and potato apyrase

Analogues **2b**–**5b** were evaluated as either substrates or inhibitors of Nucleoside Triphosphate Diphosphohydrolase, NTPDase1, and of potato apyrase (equivalent enzyme to NTPDase1). Previously, we reported that analogues **2b** and **3b** were poor substrates of NTPDase1 at 100 μM, with hydrolysis of 31% and 20% of the comparable ATP rate.[9] Here, analogues **4b**–**5b** (100 μM) were evaluated as bovine spleen NTPDase1 substrates and were also found to be poorly hydrolyzed by NTPDase1, with 14% and 23% the rate of ATP, respectively (data not shown). To further determine the interaction of analogues **4b** and **5b** with NTPDase1, we evaluated the influence of these analogues on the ATP hydrolysis rate. At a low concentration (10 μM), these analogues

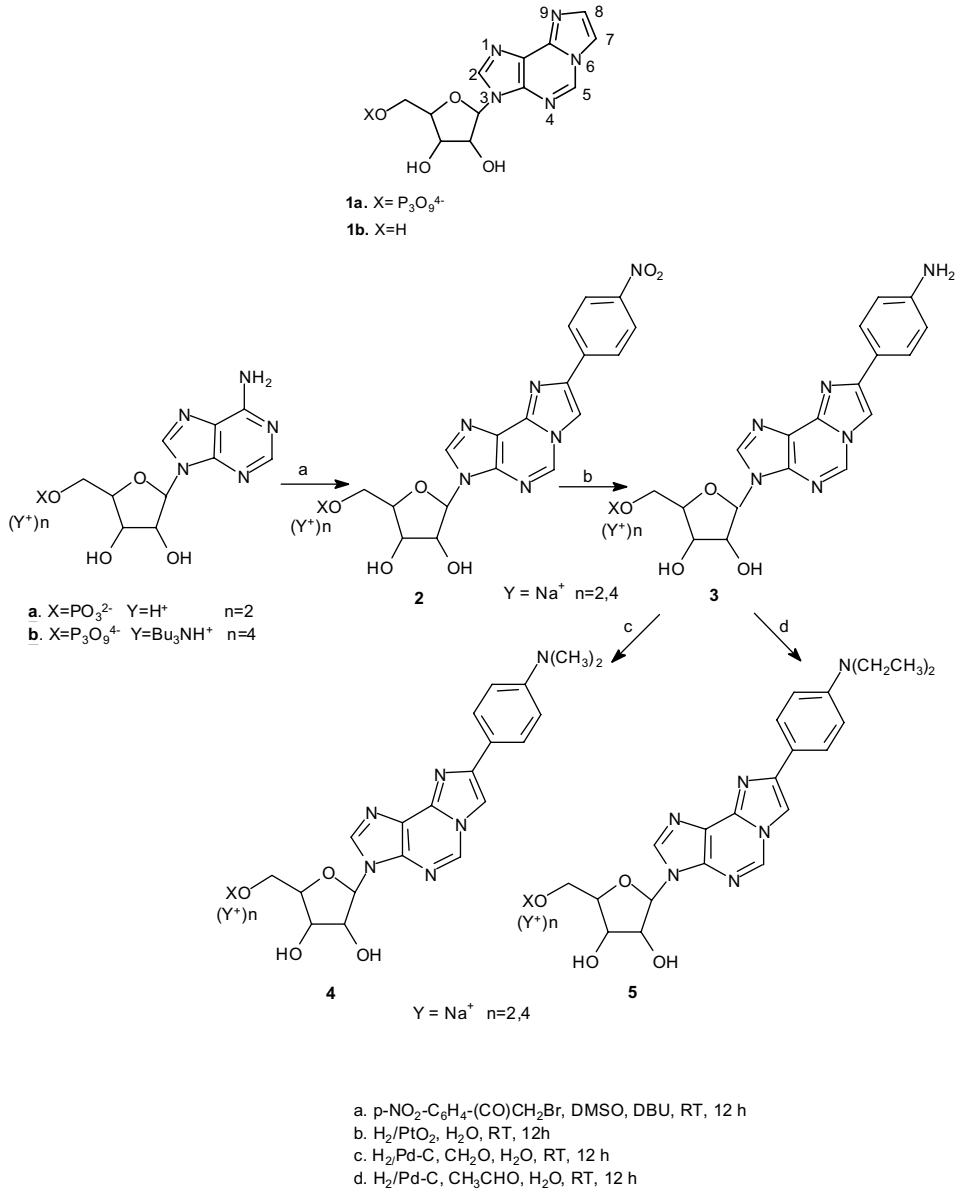

Scheme 1. The synthesis of analogues **2a**,**b**–**5a**,**b** from the corresponding adenine nucleotides.

exerted no significant inhibition of ATP hydrolysis, while only small inhibition was observed at 75 μM, with 31% and 16% inhibition for **4b** and **5b**, respectively (data not shown). These results indicate that either affinity or V_{max}, or both, would be lower than those of ATP.

In a second series of experiments, analogues **3b**–**5b** were evaluated on potato-apyrase (Fig. 2). Potato-apyrase was chosen for these studies because it exhibits similar activity to NTPDase1, and has 20–29% identity to known mammal NTPDases. Yet, practically, potato-apyrase is much easier to study because, unlike NTPDase1, it is water soluble and stable.[17]

As for NTPDase1, all analogues were found to be poor substrates of potato apyrase with 12%, 13%, and 37% hydrolysis for **3b**, **4b**, and **5b**, respectively, as compared to the rate of ATP (Fig. 2). A more detailed analysis was performed and kinetic parameters for **5b** and ATP were determined. The $K_{m,app}$ of **5b**, 45 μM, was close to $K_{m,app}$ of ATP, 37 μM, while their V_{max} were different, 304 μmol Pi/min/mg protein compared to 770 μmol Pi/min/mg protein. The comparable $K_{m,app}$ values for **5b** and ATP, indicate that they have a similar affinity for the catalytic site.

The weakest substrates were studied as inhibitors of apyrase. Thus, analogues **3b** and **4b** inhibited the hydrolysis of ATP, at 100 μM concentration of both substrate and inhibitor, by 25% and 33%, respectively.

2.5. Spectral investigation of probe 3b

Out of the series of ε-ATP derivatives **2b**–**5b**, compound **3b** was found suitable for elucidating the physicochemical properties of $P2Y_1$-R. Therefore, here, we focused on

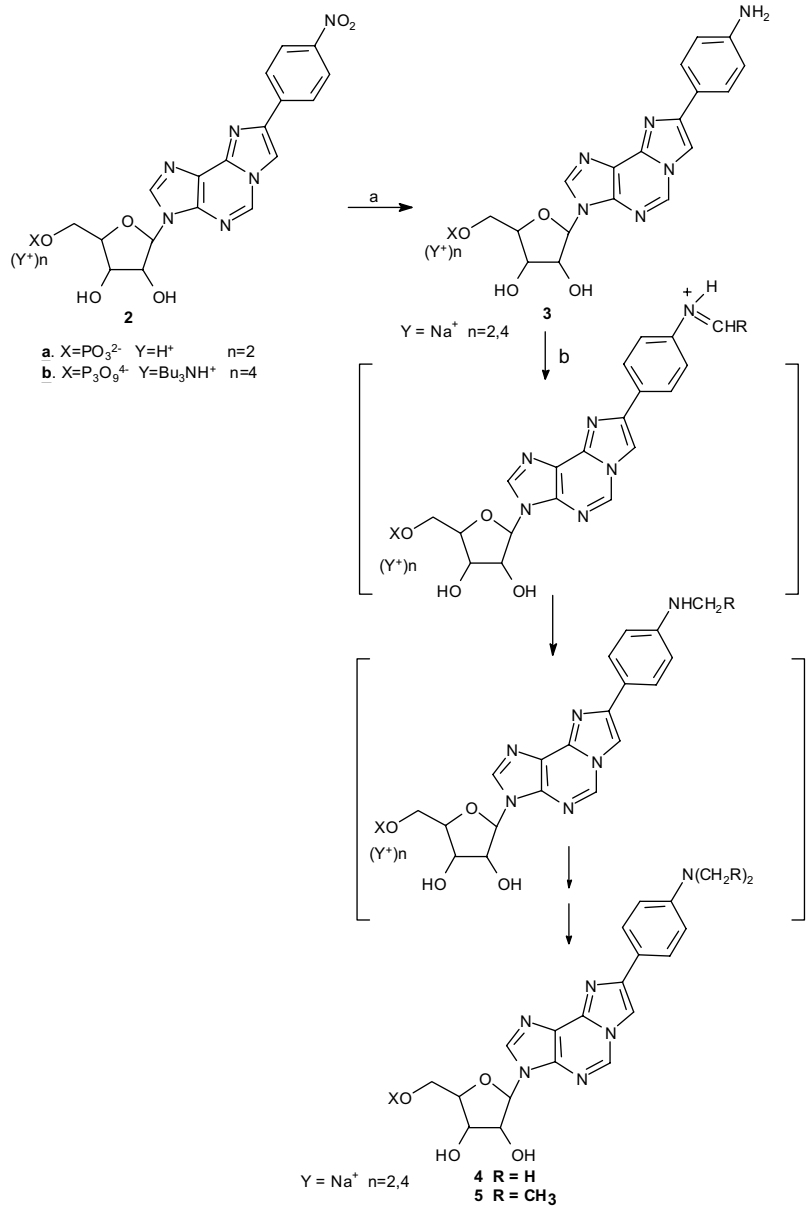

Scheme 2. The mechanism of formation of analogues **3**–**5** from analogue **2**.

a detailed spectral investigation of **3b**, with a view to establish correlation equations for elucidation of the target protein properties.

2.6. Absorption spectroscopy of probe 3b

The substitution of the aryl group on the ε-bridge in analogue **3b**, causes a significant shift in the absorption spectra, as compared to the spectrum of ε-ATP. λ_{max} shifts from 294 nm for ε-ATP[8b] to 331 nm for **3b**, at neutral pH (Table 1). Moreover, the extinction coefficients of **3b** are up to 5-fold higher as compared to those of the parent ε-ATP.[8b] The UV absorptions of **3b** are pH-dependent. In a basic medium (pH 12.3), no change is observed in λ_{max} and ε of **3b** as compared to those values at pH 7. However, in an acidic medium (pH 1.6), in which the nucleotide is still stable for several hours,[9] a pronounced blue shift of 50 nm was observed in the UV spectrum of **3b** upon shift from pH 7 to 1.6. This blue shift is due to the absorption of protonated **3b** species (discussed below).

The UV absorptions of **3b** depend also on the polarity of the medium. Thus, UV spectra of **3b** in a variety of organic solvents of comparable viscosity but increasing dielectric constants, from dioxane (2.2) to DMSO (46.7), resulted in a ca. 12-fold increase of the absorption (Fig. 3A, partial spectrum). Likewise, red shifts of ca. 10 nm were observed for spectra of **3b** in polar solvents (DMF and DMSO), as compared to the spectra in nonpolar solvents (dioxane, CH_2Cl_2, and $CHCl_3$).

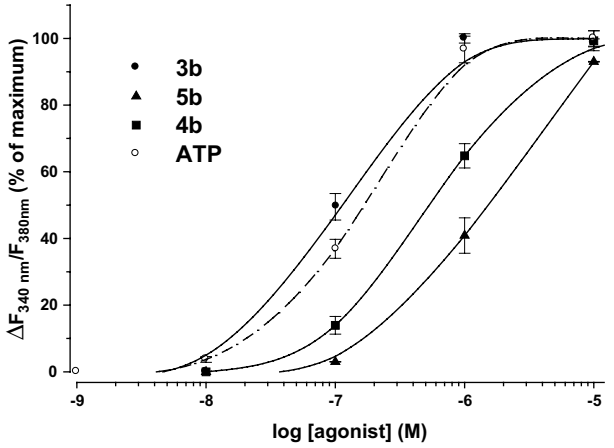

Figure 1. Evaluation of analogues **3b**–**5b** as $P2Y_1$-R agonists. Concentration–response curves for ε-ATP analogues **3b**–**5b**, and ATP, by measuring Ca^{2+} release in HEK 293 cells expressing the rat brain $P2Y_1$ receptor. The potency of the substances indicated to raise the fluorescence ratio ($\Delta F_{340nm}/F_{380nm}$) was determined as described in Methods. EC_{50} value obtained for ATP is 200 nM, for **3b** 100 nM, for **4b** 500 nM and for **5b** 1.5 μM. Data represent the mean values and standard errors from 60 to 100 single cells from at least three separate experiments.

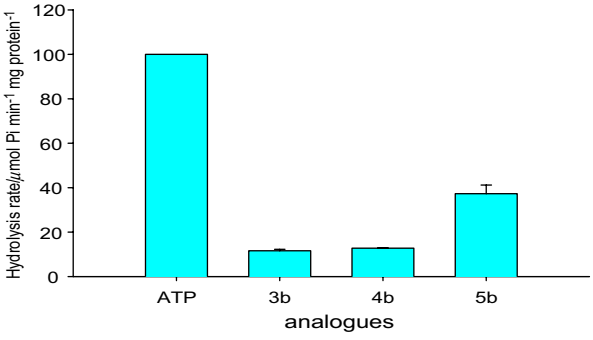

Figure 2. Hydrolysis of ATP and analogues **3b**–**5b** by potato-apyrase. ATP and analogues were used at a concentration of 100 μM. Hydrolysis was performed at 37 °C for 7 min in the presence of 5.5 μg of protein. Results are expressed as the mean SEM of two replicates performed in duplicate (**3b**: 11.6 ± 0.675, **4b**: 12.78 ± 0.061, **5b**: 37.3 ± 3.87).

Table 1. Absorption and emission data of analogue **3b** in aqueous solutions at concentrations of $1–3 \times 10^{-5}$ M

pH	Absorption	Emission	
	λ_{max} (nm) ($\varepsilon \times 10^{-3}$)	λ_{max} (nm)	ϕ
1.6	250 (**24.5**), 281 (**18.6**)	412	0.440
7.0	274 (**25.2**), 331 (**5.8**)	418	0.020
12.3	274 (**25.6**), 333 (**5.5**)	420	0.005

The absorbance of spectra of **3b** in a series of alcohols of comparable viscosity was linearly dependent on the polarity of the alcohol (Fig. 3B). Yet, no polarity-dependent shift was observed for λ_{max} of **3b**. H-bonding stabilization in these protic solvents resulted in high absorptions even at dielectric values lower than those of DMF and DMSO.

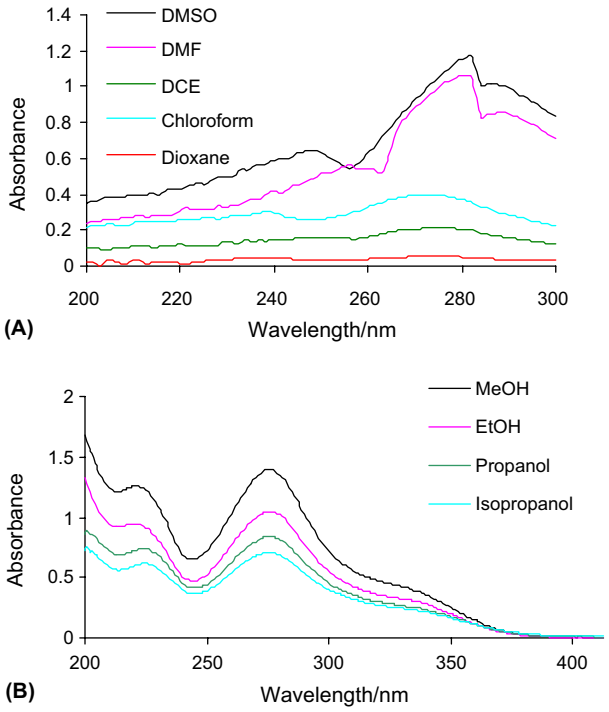

Figure 3. UV absorption spectra of **3b** tetrabutylammonium salt (4.98×10^{-5} M) in: A. Aprotic organic solvents with the following dielectric constants: DMSO 46.7, DMF 36.7, DCE 10.2, $CHCl_3$ 4.6, dioxane 2.2 (partial spectrum). B. Protic organic solvents with the following dielectric constants: MeOH 32.6, EtOH 24.3, propanol 20.1, isopropanol 18.3.

2.7. Emission spectroscopy of probe 3b

The pH-dependence of the emission spectra of analogue **3b** was investigated with a view to use it as an acidity probe. Thus, emission maxima and quantum yields (ϕ) were measured for **3b** at acidic, neutral, and basic pH (Table 1). Excitation of **3b** was performed at 290 nm,[9] and emission maximum was observed at 420 and 418 nm in basic and neutral solutions, respectively. In acidic medium, the emission maximum further shifted to 412 nm, however, fluorescence intensity increased significantly. A quantum-yield enhancement of ca. 90-fold was observed at pH 1.6, as compared to the yield in basic pH. The pH-dependence of **3b** is exceptional as compared to the vanishing fluorescence of **2b**[9] or ε-adenosine,[8b,18] **1b**, and ε-ATP,[19] **1a**, at acidic pH.

Stokes shifts of ca. 90 nm (13 kcal/mol) are observed at all pH values. These red-shifts are due to the strong interaction of the polar excited state with the polar solvent, in addition to other possible relaxation mechanisms.

2.8. Probe 3b is pH-sensitive

The dependence of the fluorescent properties of **3b** on pH was explored in detail within the pH range of 1.4–6.5 (Figs. 4 and 5). pH-titration of 1 μM solutions of **3b**, at 0.2 pH unit intervals, was monitored by fluorescence spectra at 410 nm upon excitation at 290 nm (Fig. 4).

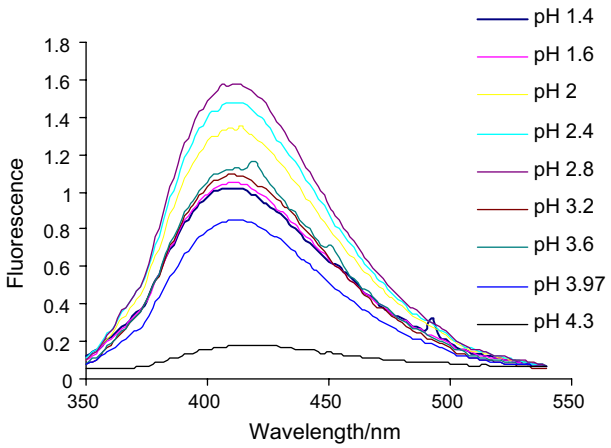

Figure 4. pH-dependence of emission spectra of probe **3b**. 1 μM solutions of probe **3b** at the pH range 1.4–4.3 were excited at 290 nm, and fluorescence intensity was measured at 410 nm.

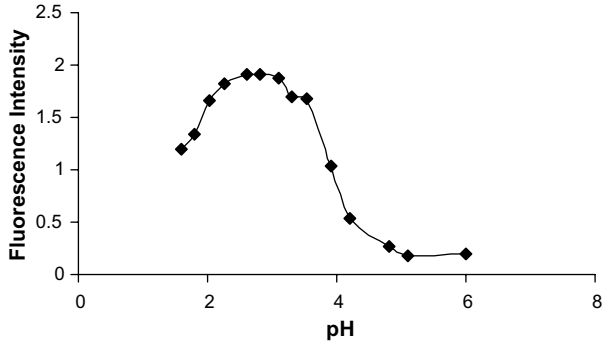

Figure 5. A bell-shaped pH-titration curve of probe **3b**. pH-titration was monitored by emission spectra (excitation at 290 nm; emission maximum at 410 nm). Three inflection points are found over the pH range of 1.5–6.0 (at 2.10; 3.09; and 3.82).

A plot of fluorescence intensity versus pH shows a bell-shaped pH-dependence (Fig. 5). Although significant fluorescence intensity was observed for **3b** at pH 1.4 (ϕ 0.44, resulting from the tri-protonated **3b**, as discussed below), the maximal emission was observed at pH 2.8 (ϕ 0.75, resulting from the di-protonated **3b**). A significant reduction of emission intensity was observed upon pH increase from pH 4.0 to 4.3. From pH 4.3 onwards no significant change is observed in the quantum yield (ϕ 0.02). A 150-fold decrease of quantum yield is observed upon pH increase from 2.8 to 12.3 (ϕ 0.005, due to the neutral fluorophore).

The pH-sensitivity of probe **3b** is in contrast to that of ε-adenosine. The latter analogue also emitted at 415 nm, yet, at pH 2.2 its intensity was less than 10% of the intensity at pH 7.[20] Likewise, the high fluorescence intensity (ϕ 0.81) of the related 8-(N-acetylamino)-3-β-D-ribofuranosylimidazo[2,1-i]purine, was drastically reduced at pH 2 as compared to pH 7.[21]

2.9. Determination of acid–base equilibria of analogues 2b–5b

The titration curve of **3b** at the pH range 1.4–6.5 is bell shaped with three inflection points. These points correspond to three pK_a values of the fluorophore (Fig. 5).

The three pK_a values, corresponding to three basic nitrogen atoms of the fluorophore in compounds **3b**–**5b**, were determined by the second derivative of the corresponding fitted graphs.

Comparable bell-shaped titration curves were obtained for the *p*-NMe_2–, and *p*-NEt_2-phenyl-ε-ATP analogues **4b** and **5b** with three inflection points. Yet, for the *p*-NO_2-phenyl-ε-ATP analogue, **2b**, a different, two stage titration curve was obtained, corresponding to two basic nitrogen atoms in the fluorophore, with maximum fluorescence intensity at pH 4.5.

Table 2 presents the pK_a values of compounds **2b**–**5b** obtained by pH-titration monitored by emission measurements. These pK_a values are in excellent agreement with pK_a values obtained by pH-titrations monitored by UV spectroscopy (data not shown).

For analogue **2b**, only two basic nitrogen atoms were identified in the fluorophore with pK_a values of 3.86 and 1.93. Yet, for analogues **3b**–**5b**, three pK_a values were determined in the pH range of 2–4. For analogues **4b** and **5b** pK_a2 and pK_a3 values were higher than those for analogue **3b**, due to inductive effects of the alkyl groups.

For the assignment of each of the pK_a values to the corresponding basic nitrogen atom in the molecule, we monitored the pH-titration by a direct method, using ^{15}N NMR. Due to the instability of the triphosphate chain in **3b** under the experiment conditions, we chose the monophosphate homologue **3a**. Thus, 0.8 M solution of *p*-NH_2-phenyl-ε-AMP bis-(tributylammonium) salt, **3a**, in DMSO was titrated with trifluoroacetic acid (TFA) at 37 °C and ^{15}N NMR spectra were measured. Table 3 presents the chemical shifts of the fluorophore's nitrogen atoms versus number of equivalents of TFA.

Table 2. pK_a values for derivatives **2b**–**5b** obtained from fluorescence monitored pH-titration

ε-ATP-analogue	Analogue number	pK_a1	pK_a2	pK_a3
8-[*p*-NO_2-Ph]-ε-ATP	**2b**	1.93 ± 0.08	3.86 ± 0.25	—
8-[*p*-NH_2-Ph]-ε-ATP	**3b**	2.01 ± 0.19	3.09 ± 0.06	3.82 ± 0.07
8-[*p*-N(Me)$_2$-Ph]-ε-ATP	**4b**	2.05 ± 0.04	3.21 ± 0.08	4.43 ± 0.08
8-[*p*-N(Et)$_2$-Ph]-ε-ATP	**5b**	2.12 ± 0.09	3.79 ± 0.21	4.66 ± 0.16

The final value of the pK_a is given as the mean of three to five measurements ±SEM.

Table 3. Dependence of ^{15}N chemical shifts of analogue **3a** on trifluoroacetic acid concentration in DMSO

TFA (equiv)	N6	N4	N9	N1	N3	NH_2
0	−176.6	−152.8	−155.8	−140.0	−207.4	−318.6
0.2	−176.9	−152.7	−157.7	−140.2	−207.5	−319.5
0.4	−177.4	−152.0	−162.4	−140.3	−207.5	−320.1
0.8	−181.9	−149.6	−178.9	−140.4	−206.7	−322.4
1.2	−183.8	−148.7	−179.7	−140.6	−206.3	−324.8

After the addition of 1.2 equiv of TFA, the N9 signal shifted upfield by 24 ppm due to protonation, while the N6 and NH_2 signals shifted upfield by 7 and 6 ppm, respectively. The most basic position of the fluorophore is N9 with pK_a of 3.82 for **3b**. This value is 0.5 log unit lower than the value reported for ε-ATP.[20b] The reduction of the basicity of N9 is expected due to the extension of the fluorophore, and the subsequent reduction of the availability of the N9 lone pair. The reduction of the pK_a value of the *p*-amino moiety (3.1 in **3b**) as compared to aniline (pK_a 4) is explained by similar considerations. N6 is the least basic nitrogen with pK_a 2.0. The basicity of nitrogens N7; N3; N1 is negligible.

Indeed, X-ray crystallography of 7-ethyl-ε-adenosine hydrochloride,[22] and ^1H NMR data for ε-AMP indicated that N9 is the primary protonation site.[23] However, the pK_a value corresponding to N6 was not reported before.

2.10. Probe 3b is viscosity sensitive

The dependence of the emission spectra of probe **3b** on the viscosity of the medium was measured within the viscosity range of 16–245 cP in ethylene glycol: glycerol mixtures of various ratios (Fig. 6). Emission maximum, λ_{max}, remained constant, 494 nm, in the entire range of viscosities. Yet, a significant increase of fluorescence intensity was observed in viscous media (Fig. 6A). A linear relationship was found between log ϕ and log viscosity (Fig. 6B).

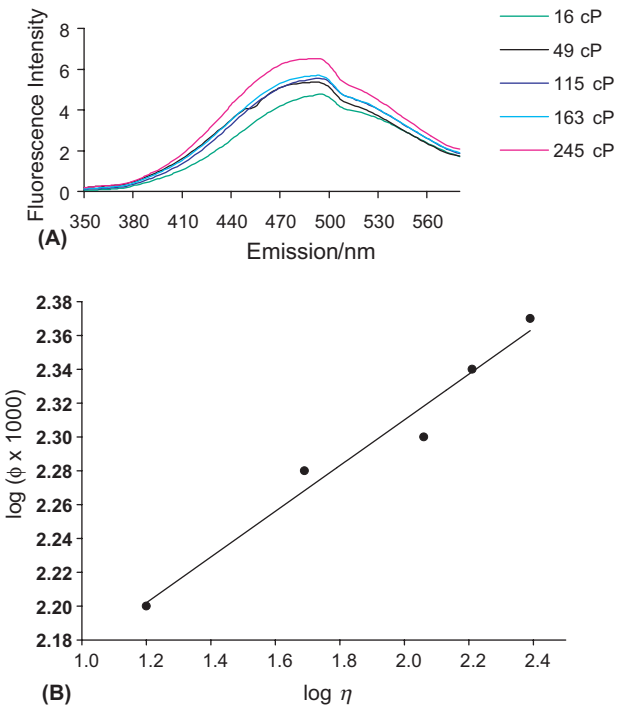

Figure 6. Dependence of emission spectra of probe **3b** on the viscosity of the medium. (A) Emission spectra were measured for 1 μM solutions of **3b** in ethylene glycol/glycerol mixtures of varying viscosities within the range of 16–245 cP. Emission maximum remains constant in the entire range of viscosities. (B) A linear relationship was found between log quantum yield and log viscosity, R^2 0.96.

2.11. Probe 3b is dielectricity sensitive

The responsiveness of probe **3b** to the dielectricity of the medium was evaluated regarding the solvation mechanism by both dipole–dipole interactions and H-bond network. In aprotic media, dipole–dipole interaction is the predominant solvation mechanism. Yet, in protic solvents, in addition to dipole–dipole interaction, an efficient solvation mechanism is the H-bond network. Therefore, emission spectra of **3b** were measured in sets of protic and aprotic solvents (Fig. 7). The set of aprotic solvents included dioxane, chloroform, dichloroethane, DMF, and DMSO, with dielectric constants in the range of 2–47. The other set included protic solvents: isopropanol, propanol, ethanol, and methanol, with dielectric constants in the range of 18–33.

A linear correlation was observed between the dielectric constant of aprotic solvents, and both λ_{max} and ϕ of **3b** (Fig. 7C, R^2 0.95, and Table 4). For aprotic solvents, by increasing the dielectricity from 2.2 (dioxane) to 46.7 (DMSO), the quantum yield is dramatically increased from 0.01 to 0.68. This supports the role of dipoles of the polar solvent in the stabilization of the excited state of the fluorophore. Furthermore, by increasing the dielectricity from dioxane to DMSO, the fluorescence emission maximum of **3b** shifts to longer wavelengths, from 416 to 476 nm. This red-shift results primarily from solvent stabilization of the excited charge-transfer state where $\mu_e > \mu_g$.

For the series of alcohol solvents, an increase of the dielectricity from 18.3 (*i*-PrOH) to 32.6 (MeOH) causes an increase of the quantum yield from 0.18 to 0.39 (Table 5). The significant stabilization of the excited state of the fluorophore by H-bonds is indicated by the high quantum yield, even at relatively low dielectric constants (*i*-PrOH). A linear correlation was observed also between the dielectric constants of alcohols and λ_{max} of **3b** in these solvents (Fig. 7C, R^2 0.97). H-bonding stabilization is also implied by the emission maxima of **3b** in alcohols, 474–496 nm, as compared to λ_{max} in polar and nonpolar aprotic solvents (Tables 4 and 5).

The curves for λ_{max} of **3b** in protic and aprotic solvents of different dielectric constants have similar slopes, 1.30 and 1.26 nm/ε_d, respectively, and are separated by about 33 nm (Fig. 7C). This separation corresponds to an energy difference of 4.9 kcal/mol, due to additional stabilization of the excited state of **3b** by H-bonds, in protic solvents.

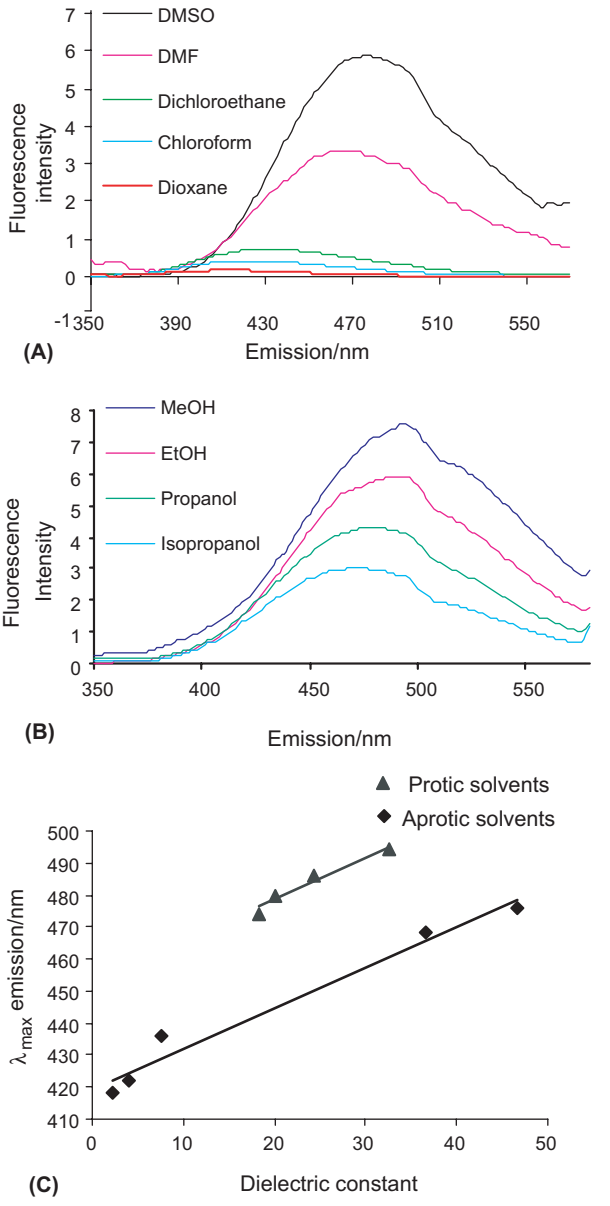

Figure 7. Dependence of fluorescence intensity of probe **3b** on the dielectric constant of the medium. (A) Dependence on dipole–dipole interactions in aprotic solvents with dielectric constant range of 2–47. (B) Dependence of fluorescence intensity of probe **3b** on the dielectric constant and H-bonding properties of the medium, using alcohols with dielectric constant range of 18–33. (C) Dependence of emission maximum of probe **3b** on the dielectric constant (▲) and on the dielectric constant and H-bonds (■) of the solvents series (R^2 0.95, 0.97).

Table 4. Fluorescence properties of probe **3b** as a function of dielectric constant of the medium

Solvent	Dielectric constant (ε_d)	λ_{max}	ϕ
DMSO	46.7	476	0.682
DMF	37.6	468	0.330
DCE	10.2	432	0.032
Chloroform	4.6	422	0.022
Dioxane	2.2	416	0.011

Table 5. Fluorescence properties of probe **3b** as a function of dielectric constant and H-bonding of the medium

Solvent	Dielectric constant (ε_d)	λ_{max}	ϕ
Methanol	32.6	496	0.391
Ethanol	24.3	488	0.291
Propanol	20.1	480	0.238
Isopropanol	18.3	474	0.183

The strong dependence of the emission spectra of **3b** on H-bonds results from specific solvent-probe interactions. These specific interactions possibly involve H-bonds with NH_2, N9, N1, and N6.

2.12. Probe 3b is sensitive to interacting acidity and dielectricity/H-bonding parameters

A pK_a value of an amino-acid residue in a protein is highly dependent on the dielectricity of its microenvironment. The formation of H-bonding network is also polarity dependent.

Therefore, we evaluated the dependence of the fluorescence spectra of probe **3b** on the correlated variables—dielectricity, H-bonding, and acidity. For this purpose, 1.9 μM solutions of **3b** in various alcohols (MeOH, EtOH, PrOH, *i*-PrOH) with dielectric constants ranging from 33 to 18, were titrated with TFA, up to 3 equiv. The titration curves show three inflection points (three 'pK_a-like' values) similar to the curves obtained by pH-titration (Fig. 5). The inflection points are expressed in terms of number of equivalents of TFA (Table 6, panel A). The number of TFA equivalents is converted to 'virtual' pK_a values in water, considering the self-association of TFA, to give 'pK_a-like' values of **3b** (Table 6, panel B).

An inverse relationship is observed between the dielectricity of an alcohol, and the 'pK_a-like' of probe **3b**

Table 6. Correlation between dielectric/H-bonding and acidity

Solvent	Inflection point 1	Inflection point 2	Inflection point 3
A			
MeOH	0.38 ± 0.14	1.36 ± 0.11	2.19 ± 0.10
EtOH	0.28 ± 0.09	0.93 ± 0.08	1.80 ± 0.11
Propanol	0.26 ± 0.10	0.88 ± 0.25	1.76 ± 0.03
Isopropanol	0.23 ± 0.15	0.79 ± 0.10	1.73 ± 0.06
	'pK_a-like'1	'pK_a-like'2	'pK_a-like'3
B			
MeOH	4.72	4.17	3.96
EtOH	5.15	4.63	4.34
Propanol	5.35	4.83	4.52
Isopropanol	5.41	4.87	4.53

Solutions of probe **3b** in MeOH, EtOH, propanol, and isopropanol were titrated with trifluoroacetic acid and monitored by fluorescence spectra (Fig. 8). (A) The inflection points of the acid-titration graphs are expressed in terms of number of TFA equivalents. The final number of TFA equivalents is given as the mean of three measurements ±SEM. (B) 'pK_a-like' values of **3b** are given in terms of 'virtual' pK_a values in water.

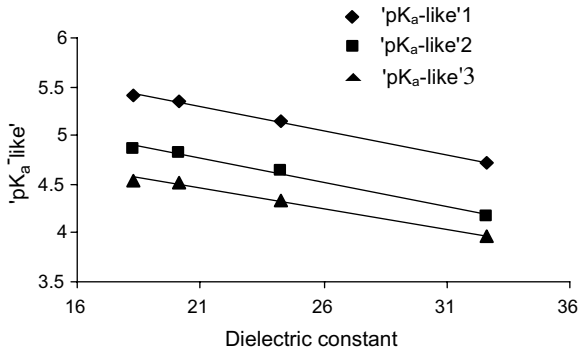

Figure 8. Dependence of fluorescence intensity of probe **3b** on the correlation between dielectricity/H-bonding and acidity. Solutions of **3b** in alcohols were titrated with 0–3 equiv TFA. Three inflection points were obtained for **3b**, providing the 'pK_a-like' values (Table 6). This graph represents one of three measurements. The final value of the pK_a is given as the mean of the three measurements ±SEM (Table 6). 'pK_a-like' values decrease as the dielectric constant increases (R^2 0.98–0.99).

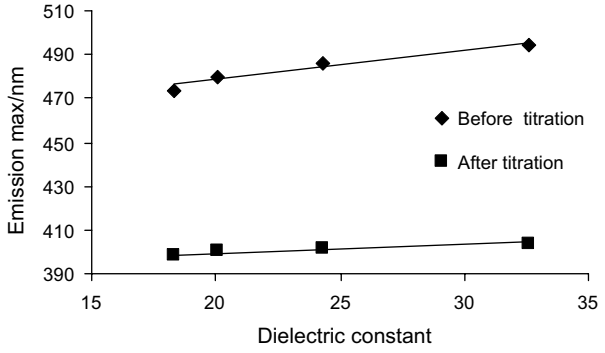

Figure 9. Emission maxima of probe **3b** versus dielectric constants of the medium, before and after titration with TFA (R^2 0.92, 0.94).

(Fig. 8). All nitrogen atoms of the probe become less basic as dielectricity increases. An increase of ca. 1 log unit, is observed for all 'pK_a-like' values in MeOH (Table 6, panel B), as compared to those values in water (Table 2).

A plot of the emission maxima of **3b** in alcohols versus the dielectric constants of these alcohols, before and after acid titration, shows two linear curves with increasing separation (Fig. 9). This large separation of up to 95 nm, is due to specific interactions of the acid-containing solvent with the probe. The blue-shift observed here for acid titration of **3b** in the alcohol series is in accordance with the same shift observed with pH-titration of **3b** (shift from 420 to 408 nm). The shift is more pronounced in alcohols possibly due to the better stabilization of the hydrophobic fluorophore in alcohols, as compared to water.

2.13. Probe 3b is sensitive to interacting acidity and viscosity parameters

The acidity and H-bonding network within a protein binding pocket is expected to be dependent also on the viscosity that affects the reorientation of the dipoles at that site. For the estimation of the dependence of protonation and H-bonding equilibria on the viscosity of the medium, we measured fluorescence spectra of probe **3b** in solutions of constant dielectricity, but varying viscosity, with the gradual addition of TFA. Probe **3b** was dissolved in ethylene glycol: glycerol solutions in differing ratios, giving rise to viscosities within the range of 16–245 cP (Fig. 10). The inflection points of the acid-titration graphs are expressed in terms of number of TFA equivalents (Table 7, panel A), and also expressed as 'pK_a-like' values in water, considering the self-association of TFA (Table 7, panel B). A linear relationship is observed between the viscosity of the medium and the pK_a1/2/3 values of **3b** (Fig. 11). As for the correlation between dielectric/H-bonding and acidity, a significant $\Delta\lambda_{max}$, up to 96 nm, is observed upon acid titration of **3b** in viscous solvents (Table 8). This blue-shift is due

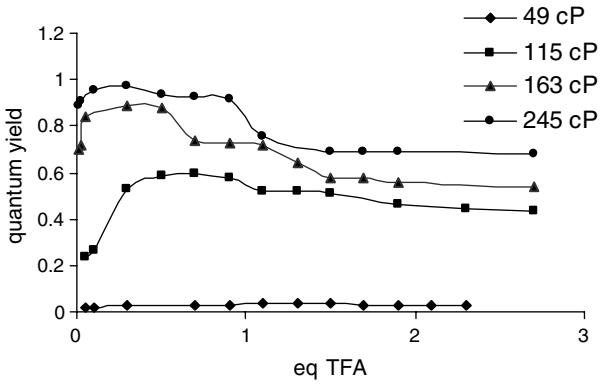

Figure 10. Dependence of the quantum yield of **3b** on the correlation between viscosity and acidity. 1 μM solutions of **3b** in ethylene/glycol mixtures of varying viscosities in the range of 16–245 cP were titrated with TFA. This graph represents one of three measurements. The final value of the 'pK_a-like' is given as the mean of the three measurements ±SEM (Table 7).

Table 7. Correlation between viscosity and acidity

Viscosity (cP)	Inflection point 1	Inflection point 2	Inflection point 3
A			
49	1.64 ± 0.01	0.98 ± 0.03	0.21 ± 0.03
115	1.54 ± 0.13	0.86 ± 0.07	0.14 ± 0.04
163	1.35 ± 0.02	0.72 ± 0.07	0.10 ± 0.005
245	1.18 ± 0.10	0.65 ± 0.02	ND[a]
	'pK_a-like'1	'pK_a-like'2	'pK_a-like'3
B			
49	4.50	4.73	5.40
115	4.53	4.78	5.57
163	4.59	4.86	5.72
245	4.64	4.90	ND[a]

Solutions of probe **3b** in the following viscosities were titrated with trifluoroacetic acid and monitored by fluorescence spectra (Fig. 10). (A) The inflection points of the acid-titration graphs are expressed in terms of number of TFA equivalents. The final number of TFA equivalents is given as the mean of three measurements ±SEM. (B) 'pK_a-like' values of **3b** are given in terms of 'virtual' pK_a values in water.

[a] ND=not detectable.

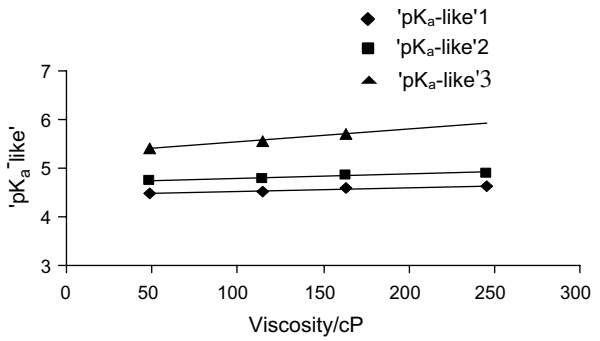

Figure 11. The dependence of 'pK_a-like' values of **3b** on the viscosity of the medium (R^2 0.95–0.99).

Table 8. λ_{max} Differences of probe **3b** in viscous solvents before and after acid titration

Viscosity (cP)	$\Delta\lambda_{max}$ (nm)
49	90
115	92
163	92
245	96

to specific interactions of the acid-containing solvent with **3b**.

3. Discussion

3.1. Biochemical relevance of the new fluorescent probes

Extracellular ATP serves as an important signaling molecule in many physiological processes.[24] ATP effects are mediated by a ubiquitous family of nucleotide receptors known as P2 receptors (P2-Rs). All P2X-Rs, that are ion-gated channels, and several P2Y-Rs, that are G-protein-coupled-receptors, respond to ATP.[25] We, and others, computed a model of the $P2Y_1$-R and established the molecular recognition determinants of agonists in the $P2Y_1$-R.[26–28] However, experimental data on the 3D structure of the binding site of P2-Rs are still lacking. Moreover, no information is available on the physicochemical properties of the P2Y-Rs binding site. The lack of such data impedes the comprehension of the receptor's recognition and activation mechanisms, and the development of potent and subtype selective ligands.

Biological effects elicited by extracellular ATP are determined by P2-Rs binding affinity, and by the level of ATP present outside the cells that depends on the release of ATP and on ectonucleotidase activity. Ectonucleotidases such as NTPDase1 and 5′-nucleotidase are major enzymes responsible for the hydrolysis of extracellular nucleoside triphosphate.[29] The presence of NTPDase1 in the vicinity of P2-R was suggested indicating its possible role in modulating nucleotides level to avoid receptor desensitization.[30] NTPDase1 catalyzes the sequential hydrolysis of phosphate γ, and β of nucleoside tri- and diphosphate, in the presence of Ca^{2+} or Mg^{2+}.[31] Only limited information is available on the properties of NTPDases binding site. Few chemical modifications[32] or site-directed mutagenesis studies showed important amino acids and a sequence corresponding to phosphate binding motifs.[33] The physicochemical characteristics of the NTPDase binding site are still unknown.

To elucidate the physicochemical properties of the binding site in the target proteins $P2Y_1$-R and NTPDase1, we synthesized novel fluorescent nucleotide analogues, **3**–**5**, based on the extension of the ε-ATP scaffold. The aim of the modifications of the ε-nucleotide scaffold was 3-fold: to improve fluorescence characteristics (ϕ and λ_{max}); to confer sensitivity to physicochemical properties of the medium; and to increase the affinity of the analogues for the binding site of the target proteins.

Nucleotide analogues **3**–**5** are excited at 290 nm and emit at ca. 410–420 nm, representing excitation and emission wavelengths outside the range of proteins absorption and emission spectra. In addition, the sensitivity of the detection of these analogues is relatively high (at concentrations $\leqslant 1\times10^{-6}$ M). Furthermore, analogues **3**–**5** are sensitive to changes in the acidity, polarity, H-bonding, and viscosity of the medium.

Among the new analogues, **3b** was found to be a potent $P2Y_1$-R ligand that is slightly more potent than ATP. Analogues **4b** and **5b**, presented lower affinity for the receptor, implying that **3b** *p*-NH_2 H-atoms are essential for the molecular recognition by the $P2Y_1$-R.

The major structural difference between the ε-derivatives and the natural nucleotides is masking N1 and N^6-positions. For the $P2Y_1$-R in which the ε-ATP derivative **3b** is active, the lack of free N1 and N^6 positions, known to be important for binding,[27,28] is probably compensated by favorable interactions of the *p*-amino moiety.

The affinity of analogues **3b**–**5b** to NTPDase1 and or potato apyrase, proved to be low. These analogues were poorly hydrolyzed (12–37%) and exerted little inhibition of ATP hydrolysis (16–33%) by both enzymes, as compared to ATP.

The aryl-etheno substitution is apparently unfavorable for catalytic activity. This is possibly because the bulky aryl-etheno group shifts the triphosphate moiety away from the catalytic residues, or because of the loss of H-bonding of N1 and N^6 with the enzyme.

3.2. Sensitivity of probe 3b to environmental variables

We explored the sensitivity of our probe of choice, **3b**, to environmental variables such as polarity, viscosity, acidity, and H-bonds, based on emission spectra. Furthermore, we studied the correlation between certain variables. In this way, we established the dependencies of the emission spectra of **3b**, on the interactions between the acidity and dielectricity, or the acidity and viscosity of the medium. The dependencies of **3b** on the physicochemical properties of the environment, were calibrated here by a series of solvents and solutions.

Our working hypothesis is that changes in the emission spectra of **3b** are due to the response of the probe to the environmental properties. We chose the measurement conditions to prevent unwanted effects on the emission spectra due to phenomena such as self-aggregation or metal-ion coordination.

To avoid self-association, our measurements were conducted at low concentrations, $\leqslant 1\,\mu M$, of **3b**. Furthermore, self-association in nucleoside tri-phosphates is negligible, as shown by Sigel et al., and decreases considerably from adenosine to ATP^{4-}.[34]

Generally, the presence of paramagnetic metal ion in the binding site might reduce fluorescence intensities, without shift of emission maxima (only the uncomplexed forms are fluorescent). Yet, Mg^{2+} present in various ATP-binding proteins, including our target proteins, is not paramagnetic. The binding of Mg^{2+} is not accompanied by a decrease in fluorescence intensity.[20c,35] Therefore, to avoid unwanted metal-ion coordination, we conducted the measurements with severe exclusion of paramagnetic metal ions.

3.3. pH-dependence of the emission spectra of 3b

Analogue **3b** was explored as a probe of acidity. For this purpose, we established the responsiveness of **3b** to the acidity of the medium, either in water within a wide pH-range, or in media of either varying acidity and polarity, or varying acidity and viscosity.

The absorption and emission characteristics of **3b** within the pH range 7.0–12.3 are practically the same. However, probe **3b** was found to be acid sensitive, showing a bell-shaped dependence of absorbance (not shown) and fluorescence intensity on pH in the range 1.4–6.5 (Fig. 5).

The quantum yield of **3b** was enhanced 150-fold (ϕ 0.75) upon acidification of the solution from basic or neutral pH to 2.8. However, further acidification of the solution from pH 2.8 to 1.4, resulted in a gradual decrease of fluorescence intensity (ϕ 0.44). This observation is exceptional considering the vanishing fluorescence of ε-ATP at acidic pH.[20b] To the best of our knowledge, compound **3b**, and its analogues **4b** and **5b**, are the first examples of $N1,N^6$-ε-adenine nucleotides which highly fluoresce at acidic pH. This significant enhancement of fluorescence intensity in the pH range of 1.4–4.0 suggests the possible use of **3b** as a sensor of the environment acidity.

Three basic nitrogen atoms in **3b**, N9; N6; NH_2, are responsible for the sensitivity of the probe to acidity.

Related dependence of emission spectra of fluorophore's **3b** on the acidity of the medium was observed also for nonaqueous solutions (Tables 6 and 7). Yet, the correlation between dielectricity and acidity, or viscosity and acidity, shifted the 'pK_a-like' values, as compared to water. The correlated dielectricity–acidity parameter reduced the basicity of **3b**, while the correlated viscosity–acidity parameter enhanced the basicity of **3b**, as discussed below.

3.4. Dielectricity dependence of the emission spectra of 3b

A protein is generally charged or dipolar. This polarized nature influences both the structure and function of proteins. Therefore, it is necessary to consider molecular recognition of molecules by proteins in terms of effective local dielectricity of the binding cavity.

The local dielectricity of a protein is expected to be low, as compared to the aqueous environment. The inside of a globular protein is dense with apolar atoms stabilized by the hydrophobic effect. The effect of polar groups in the binding site on dielectricity is limited due to their partial neutralization by H-bonding.[36]

Direct experimental determination of dielectricity of a protein is practically impossible. Still, the determination of dielectricity was attempted in dry powders and films of peptides and proteins by electrometric methods,[37] and by theoretical models.[38] Experimental estimates of effective dielectricity were attempted also by the analysis of the shift in pK_a of ionizable groups when they are buried in proteins.[2] These studies required the titrations of the proteins for the determination of pK_a of the buried residues. However, such titrations are applicable only for proteins that are especially stable within a wide range of pH values.

These limitations encouraged us to explore the use of **3b** also as a dielectricity probe. A linear correlation was found between the dielectricity of aprotic solvents, and the quantum yield (Fig. 7A, Table 4). The quantum yield of **3b** was increased from 0.01 to 0.68 upon increasing the dielectric from 2 to 46, thus, supporting the role of dipoles of the polar solvent in the stabilization of the fluorophore's excited state. A similar observation was made for the series of alcohol solvents (Fig. 7B, Table 5).

The effect of alcohols on the emission spectra of analogue **3b** is attributed to two distinct parameters: H-bonding and the dielectric constant. The additional contribution of H-bonds to the stabilization of the excited state of **3b**, apart from the contribution of the dielectricity, was determined as 5 kcal/mol based on graph 7C. The dependence of the emission spectra on H-bonds indicates that the red-shift of **3b** spectra in protic solvents is a result of specific solvent-probe H-bond interactions.

H-bonding equilibrium is an intermediate state in the process of protonation equilibrium. Indeed, in a more efficient H-bonding medium (i.e., MeOH vs. isopropanol), the quantum yield of **3b** is higher (Table 4). This observation is comparable to the increase of the quantum yield as the solution's pH is lowered.

Both emission maximum and quantum yield of **3b** in water (pH 7, ε_d 78) deviate significantly from those of **3b** in alcohols. λ_{max} is significantly shorter and ϕ is

significantly lower in water (418 nm, ϕ 0.02, pH 7), as compared to alcohols. This unique behavior may be due to the less efficient stabilization of the probe hydrophobic part by water, relative to alcohols.

A linear correlation was observed between the dielectric constant of protic and aprotic solvents, and λ_{max} of **3b** (Fig. 7C). The high correlation we found between these parameters (R^2 0.95 and 0.97), will be applied in our equations for the investigation of proteins, although the Lippert equation proposes a nonlinear dependence of $\Delta\nu$ on the dielectric constant.[39]

3.5. Viscosity dependence of the emission spectra of 3b

Viscosity of a protein is determined by the limited degrees of freedom of its backbone and side chains (constrained ϕ and φ angles of the peptide bond, and limitations on free rotation about bonds in side chains), and inter-residue interactions (H-bonds network, dipole–dipole interactions, etc.). Likewise, the presence of residual water molecules left in the binding cavity after ligand/inhibitor binding may affect both the local effective viscosity and dielectricity. Since the direct measurement of these microparameters within a protein is impossible, we also explored the responsiveness of probe **3b** to the viscosity of solvents.

Several molecular rotors have been developed to estimate the viscosity and dielectricity of their environment. For instance, CCVJ has been used to evaluate the specific binding to antibodies. Binding was indicated by the increase of CCVJ fluorescence due to enhanced viscosity and decreased local dielectric constant provided by the protein environment, as opposed to the aqueous solution it was dissolved in before.[40]

Likewise, several fluorescent probes were used to provide information on microviscosities and the local dielectricity of bilayers. The common assumption is that fluorescence emission characteristics can be associated with the dielectric constant of a solvent in a standard solvent scale. Yet, only a few fluorophores were reported to be capable of providing useful information on both microviscosity and local dielectricity of bilayers.[41]

The dependence of the emission spectra of probe **3b** on the viscosity of the medium was measured within the viscosity range of 16–245 cP (Fig. 6). Maximum emission, 494 nm, remained constant in the entire range of viscosities. Yet, a linear relationship was found between log quantum yield and log viscosity (Fig. 6B). This relationship is anticipated, since generally, in a highly constrained environment, the predominant decay pathway is radiative, and large increases in the fluorescence quantum yield are observed.[42]

Our observations for **3b** are in agreement with studies by Ferreira and Gratton who used ε-ATP and time-resolved fluorescence spectroscopy for the investigation of viscosity-dependent fluorescence. The rotation of the bulky adenine moiety about the glycosidic bond is expected to involve displacement of solvating molecules and thus should be dependent on viscosity.[43] Indeed, these studies supported the view that rotational diffusion of the adenine moiety in ε-ATP is linearly attenuated by the solvent viscosity.

Although the fluorescence of **3b** is viscosity dependent, **3b** is less sensitive to viscosity as compared to known molecular rotors, for example, DCVJ.[40] The sensitivity to viscosity is expressed by the slope of the line (x) of log viscosity versus log quantum yield. For instance, for DCVJ, x is 0.60, according to the Forster–Hoffmann expression for the linear relationship between quantum yield and viscosity, $\log\phi_f = C + x\log\eta$. This value agrees with the 2/3 power viscosity dependence of the quantum yield $\phi_f = C\eta^{2/3}$ for a number of dyes reported by Forster and Hoffmann.[41] For probe **3b**, the slope is 0.135, indicating a lesser sensitivity of **3b** to the viscosity of the medium, as compared to molecular rotors.

3.6. Dependence of 3b emission on the correlation between environmental variables

Generally, there is no correlation between dielectric constants and viscosities of solvents, and these two parameters are independent of each other. However, the acidity parameter, is dielectricity dependent. For instance, a pK_a value of an amino-acid residue in a protein is highly dependent on the dielectricity of its microenvironment. The acidity within a protein binding pocket is also expected to be dependent on the viscosity (i.e., on the constrained backbone, inter-residue interactions, and the presence of residual water molecules).

Therefore, we estimated the dependence of protonation equilibria of **3b** on the viscosity/H-bonding and dielectricity/H-bonding of the medium. Since both the fluorophore and the alcohol solvents are amphiprotic, it is impossible to untangle dielectricity, H-donor, and H-acceptor variables.[44] Therefore, we refer here to the correlated contribution of both dielectricity and H-bonds.

We found that indeed acid–base equilibria of **3b** are highly dependent on both dielectricity and viscosity of the medium. An inverse relationship is observed between the dielectricity of an alcohol, and the 'pK_a-like' of probe **3b**. All nitrogen atoms of the probe become less basic as dielectricity increases. This rather unexpected observation may be due to a better solvation of the relatively hydrophobic fluorophore with delocalized positive charge by more hydrophobic alcohols with longer alkyl moieties. This is in accordance with the association constants of picric acid in nonaqueous media.[45] An increase is observed for 'pK_a-like' values for the three basic nitrogens of **3b** in MeOH, as compared to those values in water. Again this observation can be rationalized by the better solvation of the hydrophobic fluorophore by MeOH, as compared to water.

Yet, acid–base equilibria of **3b** were linearly dependent on viscosity (Fig. 11).

The addition of a small amount (e.g., 0.1 equiv) of TFA to mixtures of alcohols of different viscosity and con-

stant dielectricity, induced a 92–96 nm shift of λ_{max} of **3b**. At a low concentration of acid the solution was apparently already saturated, resulting in a large shift of the emission band. The same phenomenon was observed for solutions of alcohols of different dielectricity and constant viscosity.

By adding a low concentration of TFA, too low to alter the bulk properties of the solvent, additional specific H-bonds are formed, resulting in significant blue spectral shifts of **3b**. H-bonding is essentially a chemical reaction with a typical equilibrium constant. Therefore, relatively low concentrations will saturate this specific effect.[46]

The emission of **3b** is sensitive to both specific and general solvent effects. Therefore, the use of alcohols sets to calibrate environmental properties is favorable. Firstly, because the specific effects of alcohols cause larger, easily observed spectral shifts. Secondly, identification of these specific effects in the calibration sets could reveal H-bonding of the probe within the protein binding site.

4. Conclusions

The fluorescent ε-ATP analogue **3b** is responsive to H-bonding, polarity, acidity, and viscosity of the environment. Analogue **3b** is sensitive to both specific and general effects of the solvent. This sensitivity to environmental properties and to correlation between certain properties, together with its affinity to the $P2Y_1$-receptor, makes **3b** a promising probe of the binding pocket of this protein. The dependence of the spectral parameters of **3b** on environmental parameters is summarized in Table 9. Based on these dependencies, we will establish equations correlating spectral parameters of protein-bound **3b** with environmental parameters.

Briefly, the dielectricity/H-bonding parameter in the protein may be deduced from a linear correlation with λ_{max}. Acidity, expressed as pH-function, and viscosity of the environment, may be deduced from additional equations correlating ϕ and absorbance of the protein-bound **3b** with pH-function and η (where ε_d appears as a constant found in the first equation). The equations will first be solved, by regression analysis, for **3b** in the above-described sets of solutions, and the corresponding coefficients will be deduced. Later, these equations, with known coefficients, will be applied for the analysis of the spectral data of the protein-bound sensor. These results will be published in due course.

Based on our findings we also conclude that isolating and treating one or two physicochemical properties of a biological system (proteins, nucleic acids, and membranes) by a dedicated molecular probe sensitive to one or two parameters, might be misleading due to the correlation between either acidity–dielectricity/H-bonding parameters or acidity–viscosity/H-bonding parameters. Furthermore, specific and general solvent effects for a given probe should not be separated from each other.

5. Experimental

5.1. General

New compounds were characterized and resonances assigned by proton and carbon nuclear magnetic resonance using Bruker AC-200/AC-300 NMR spectrometers. HOD signal was used as a reference, at 4.78 ppm, for samples in D_2O. Nucleotides were characterized also by ^{31}P NMR in D_2O using 85% H_3PO_4 as external reference. Nucleotide derivatives were characterized by fast atom bombardment (FAB) and high-resolution FAB using glycerol matrix under FAB negative conditions on AUTOspec-E-FISION VG high-resolution mass spectrometer. For the synthesis of analogue **2b**, ATP disodium salt, insoluble in DMSO, was converted to the corresponding ATP tetrabutylammonium salt. This conversion was performed by eluting ATP disodium salt on activated DOWEX 50WX8-200 ion-exchange resin. Purification of nucleotides was achieved on an Isco UA-6 LC system using DEAE A-25 Sephadex (HCO_3^- form) columns and a linear gradient of 0–0.5 M NH_4HCO_3. Eluting nucleotides were detected by UV absorption at 280 nm using a UV detector. The final purification of the products was achieved on an HPLC system (Merck-Hitachi) using a semi-preparative reverse-phase LichroCART lichrospher 60, RP-select B column (Merck, Darmstadt, Germany) and a linear gradient of acetonitrile (A): 0.1 M TEAA buffer (pH 7) (B) (A:B) 15:85–45:55 in 25 min (solvent system I) with a flow rate of 6 mL/min. For analytical purposes, a LiChroCART LiChrospher 60 RP-select B column (250 mm × 4 mm) was used with flow rate of 1 mL/min. The purity of the nucleotides was evaluated on an analytical column in two different solvent systems. Solvent system I, describe above, and solvent system II, consisting of 5 mM tetrabutylammonium dihydrogenphosphate (TBAP) in MeOH (A) and 60 mM ammonium dihydrogenphosphate and 5 mM TBAP in 90% H_2O/10% MeOH (B). A concentration gradient from 75% B to

Table 9. Summary of the dependence of the quantum yield (ϕ) and emission maximum (λ_{max}) values of **3b** on the environmental variables and correlated variables

	pH	Viscosity	Polarity	Polarity/H-bonding	Acidity/viscosity/H-bonding	Acidity/polarity/H-bonding
ϕ	Sigmoidal (3 curves)	Linear	Linear	Linear	Sigmoidal (3 curves)	Sigmoidal (3 curves)
λ_{max}	Sigmoidal (2 curves)	Constant[a]	Linear	Linear	Constant[b,c]	Constant[b,c]

[a] Maximum emission appears at 494 nm at all viscosities.
[b] Maximum emission is almost constant during acid titration per certain viscosity or dielectricity.
[c] A large λ_{max} difference of **3b** of 92–96 nm is obtained upon the addition of 0.1 equiv TFA to a medium of a certain viscosity or dielectricity.

25% B in 20 min was applied. Triethylammonium salts of mono- and tri-nucleotides, obtained after HPLC separation, were treated with SEPHADEX-CM C-25 and converted in this way to the corresponding di- or tetra-sodium salts. Compounds **2a**,**b** and **3a**,**b** were prepared as described previously.[9] Triethylammonium salts of nucleotides **2**–**5** obtained after HPLC separation were converted to the corresponding di- or tetra-sodium salts with SEPHADEX-CM C-25 prior to spectral measurement. For the measurement of emission spectra of the nucleotides in organic solvents, the counter ion was exchanged from tetra-ethylammonium to tetra-butylammonium by Chelex-100 (Bu_4N^+)-form column. This column was prepared as follows: Chelex-100-Na^+ 100–200 mesh resin (1.5 mL) in a column, was washed with an aqueous solution of tetrabutylammonium bromide (at least 3 equiv). The column was then washed with deionized water (90 mL). Spectroscopic grade ethylene glycol and glycerol were used. Freshly distilled spectroscopic grade trifluoroacetic acid was used for acid titrations in organic solvents.

5.1.1. 8-(*p*-N,N-dimethylamine-phenyl)-3-β-D-ribofuranosylimidazo[2,1-i]purine-5-triphosphate, 4b, 8-(*p*-N,N-diethylamine-phenyl)-3-β-D-ribofuranosylimidazo[2,1-i]purine-5-triphosphate, 5b. Typical procedure. A solution of **2b** (20 mg, 0.027 mmol) in H_2O (5 mL) and 40% aqueous acetaldehyde (100 μL), was subjected to hydrogenation over Pd–C catalyst at 55 psi overnight, at room temperature.

Compound **4b**. TLC (*iso*-propanol/H_2O/NH_4OH, 65:30:5) indicated that the reaction was completed after 12 h, showing a typical spot at R_f 0.36. After removal of the catalyst by filtration, the product was purified by HPLC. Retention time of **4b** was 12.19 min in solvent system I (purity > 98%), and 12.40 min in solvent system II (purity > 96%). Product **4b** was obtained after repeated freeze-drying cycles in 85% yield (19.9 mg). ^{1}H NMR (300 MHz, D_2O, pH 8.5) δ: 9.12 (s, 1H, H-5), 8.70 (s, 1H, H-7), 7.71 (ABq, 2H, Ar), 7.09 (ABq, 2H), 6.33 (d, 1H, H-1′), 4.73 (t, 1H, H-2′), 4.48 (t, 1H, H-3′), 4.16 (q, 1H, H-4′), 3.88 (2H, H-5′), 2.98 (s, CH_3) ppm. ^{31}P NMR (200 MHz, D_2O, pH 6) δ: −9.0 (d), −10.7 (d), −21.3 (t) ppm. FAB (negative mode) *m*/*z*: 649.602 ($M^{4-} + 3H^+ + Na^+$); HRFAB: calcd for $C_{20}H_{24}N_6O_{13}P_3$ 649.362, found 649.063.

Compound **5b**. TLC indicated that the reaction was completed after 12 h, showing a typical spot at R_f 0.39. After removal of the catalyst by centrifugation, the product was purified by HPLC. Product **5b** was eluted out of the HPLC column with retention time of 16.11 min in solvent system I (purity > 98%), and 16.80 min in solvent system II (purity > 95%). Product **5b** was obtained after repeated freeze-drying cycles in 87% yield (17.9 mg). ^{1}H NMR (200 MHz, D_2O, pH 6) δ: 9.04 (s, 1H, H-5), 8.64 (s, 1H, H-2), 8.18 (s, 1H, H-7), 7.87 (ABq, 2H, Ar), 6.92 (ABq, 2H), 6.31 (d, 1H, H-1′), 4.47 (t, 1H, H-2′), 4.32 (t, 1H, H-3′), 4.18 (q, 1H, H-4′), 4.10 (2H, H-5′), 3.42 (q, 4H, CH_2), 1.16 (t, H, CH_3) ppm.^{31}P NMR (200 MHz, D_2O, pH 6) δ: −5.5 (d), −10.4 (d), −21.2 (t) ppm. FAB (negative mode) *m*/*z*: 677.151 ($M^{4-} + H^+ + Na^+$); HRFAB: calcd for $C_{22}H_{28}N_6O_{13}P_3$ 677.414, found 677.092.

5.1.2. 8-(*p*-N,N-dimethylamine-phenyl)-3-β-D-ribofuranosylimidazo[2,1-i]purine-5-monophosphate, 4a, 8-(*p*-N,N-diethylamine-phenyl)-3-β-D-ribofuranosylimidazo[2,1-i]-purine-5-monophosphate, 5a. Typical procedure. A solution of **2a** (20 mg, 0.038 mmol) in H_2O (5 mL) and 40% aqueous acetaldehyde (140 μL), was subjected to hydrogenation over Pd–C catalyst at 55 psi overnight, at room temperature.

Compound **4a**. TLC (*iso*-propanol/H_2O/NH_4OH, 65:30:5) indicated that the reaction was completed after 12 h, showing a typical spot at R_f 0.63. After removal of the catalyst by filtration, the product was purified by HPLC. Retention time of **4a** was 15.01 min in solvent system I (purity > 96%), and 2.96 min in solvent system II (purity > 93%). The product yield was 89% (18mg). ^{1}H NMR (300 MHz, D_2O, pH 6) δ: 8.91 (s, 1H, H-5), 8.78 (s, 1H, H-7), 7.20 (ABq, 2H, Ar), 6.69 (ABq, 2H), 6.33 (d, 1H, H-1′), 4.81 (t, 1H, H-2′), 4.58 (t, 1H, H-3′), 4.44 (q, 1H, H-4′), 4.10 (2H, H-5′), 2.67 (s, CH_3) ppm.^{31}P NMR (200 MHz, D_2O, pH 6) δ: 4.6 (s) ppm. FAB (negative mode) *m*/*z*: 649.602 ($M^{4-} + 3H^+ + Na^+$); HRFAB: calcd for $C_{20}H_{22}N_6O_7P$ 489.406, found 489.130.

Compound **5a**. TLC showed a typical spot at R_f 0.88. After removal of the catalyst by centrifugation, the product was purified by HPLC. Product **5a** was eluted out of the HPLC column with retention time of 18.37 min in solvent system I (purity > 95%), and 3.17 min in solvent system II (purity > 94%). Product **5a** yield was 83% (17.7mg) after repeated freeze-drying cycles. ^{1}H NMR (200 MHz, D_2O, pH 8.5) δ: 8.57 (s, 1H, H-5), 8.43 (s, 1H, H-2), 7.45 (s, 1H, H-7), 6.80 (ABq, 2H, Ar), 6.04 (ABq, 2H), 5.80 (d, 1H, H-1′), 4.51 (t,1H, H-2′), 4.37 (t, 1H, H-3′), 4.14 (q, 1H, H-4′), 3.68 (2H, H-5′), 3.21 (q, 4H, CH_2), 1.36 (t, H, CH_3) ppm.^{31}P NMR (200 MHz, D_2O, pH 6) δ: 1.8 (t) ppm. FAB (negative mode) *m*/*z*: 561.3755 ($M^- + 2Na^+$); HRFAB: calcd for $C_{22}H_{24}N_6O_7PNa_2$ 561.123950, found 561.128304.

5.2. Absorption spectra

Spectra of compounds **2b**–**5b** were measured using a Varian array-1E UV–visible spectrometer. Spectra were determined in dilute HCl or NaOH solutions in the range of 1.4–7.0. The concentration of the samples in aqueous solutions was of the order of $1–2 \times 10^{-6}$ M, and $1 - 2 \times 10^{-5}$ M for organic solvents. Measurements were performed in 3–5 replicates, and results are expressed as the mean ± SEM.

5.3. Emission spectra

Spectra of compounds **2b**–**5b** were measured using an Aminco-Bowman series 2 Luminescence Spectrometer. Measurement conditions included: 780 V sensitivity, and a 4 or 2 nm slit in the emission spectra for aqueous or organic solutions, respectively. Emission spectra were

corrected by the subtraction of the medium's emission spectrum. Spectra were determined in dilute HCl or NaOH solutions in the pH range of 1.4–7.0. The concentration of the samples was of the order of $1–2 \times 10^{-6}$ M and $1–2 \times 10^{-5}$ M for aqueous and organic solutions, respectively. Solutions of ethylene glycol/glycerol in a range of viscosities were prepared according to literature.[40] All organic solvents were freshly distilled prior to emission measurements. Measurements of the emission of the nucleotide analogues were conducted with subtraction of the solvent's emission. The quantum yield of each compound was calculated from the observed absorbance at 290 nm and the area of the fluorescence emission band. Quinine sulfate was used as reference compound assuming a quantum yield value of 0.55.[47] Measurements were performed in 3–5 replicates, and results are expressed as the mean ± SEM.

5.4. ^{15}N NMR spectra

^{15}N NMR spectra were recorded on a Bruker DMX-600 instrument (60.8 MHz for ^{15}N) with nitromethane ($\delta = 0$) as an external standard. Negative chemical shifts are upfield from nitromethane. For TFA-titration of probe **3a** monitored by ^{15}N NMR, a 0.8 M nucleotide solution in DMSO was used. With these conditions, useful spectra could be obtained with accumulation time of 4–4.5 h. The measurement was conducted at 37 °C to enhance the nucleotide's solubility. The changes in the nitrogen shift resulting from protonation in DMSO solution were determined from the spectra. After the addition of 1.6 equiv (total) of TFA the nucleotide was no longer stable.

5.5. Calculation of pK_a

The bell-shaped graph showing pH-dependence of fluorescence spectra of **3b** (Fig. 5), was divided into three sigmoid graphs. For each of the graphs a five- or four-parameter sigmoid function was fitted to the data using SigmaPlot 2000 (SPSS, Inc.):

$$I = I_0 + \frac{a}{\left(1 + e^{-\frac{(pH - [pH]_0)}{b}}\right)^c}$$

$$I = I_0 + \frac{a}{\left(1 + e^{-\frac{(pH - [pH]_0)}{b}}\right)}$$

Where I is the fluorescence intensity. The inflection point, determined by the second derivative of the fitted sigmoid function, was the pK_a. Final pK_a values are expressed as the mean ± SEM of 3–5 measurements.

6. Biochemical assays

6.1. P2Y$_1$-receptor assays: $[Ca^{2+}]_i$ measurements

For Ca^{2+}-measurements, cells grown on coverslips were loaded for 30 min with 2 μM Fura 2-AM in HEPES buffered saline (HBS) containing 145 mM NaCl, 5.4 mM KCl, 1.8 mM $CaCl_2$, 1 mM $MgCl_2$, 25 mM glucose, and 20 mM HEPES, pH 7.4. Cells were assayed under continuous superfusion of 35 °C pre-warmed HBS (1 mL/min) in the presence of varying concentrations of different nucleotides, as indicated.

The relative enzymatic stability of the analogues tested, in addition to the fast superfusion system used to apply the different ATP analogues, precludes any appreciable enzymatic conversion. Thus, problems related to responses that may result from degraded or released nucleotides are circumvented. Constant superfusion of the pre-warmed buffer excluded unspecific Ca^{2+} responses caused by mechanical stress, temperature variation, or different components of the buffer.

Fluorescence changes of single cells were detected with an imaging system (TILL Photonics GmbH) attached to a Zeiss Axioscope, using alternate excitation at 340/380 nm and emission at 500 nm. The fluorescence emission ratio can be converted to intracellular calcium concentration $[Ca^{2+}]_i$ using the equation of Grynkiewicz et al.[48] Concentration-response data were analyzed with the EXCEL program applying $\Delta F_{340nm}/F_{380nm}$ before and after the addition of the agonist. Curve fitting was performed by using a four parameter sigmoidal equation from the regression equation library of the SIGMAPLOT program. EC_{50} values represent the agonist concentration at which 50% of the maximal effect is achieved.

6.2. Enzymatic assays

6.2.1. NTPDase assays. Reagents. ATP, tetramisole, imidazole, calcium chloride, malachite green, bovine serum albumin (BSA), and Tris-base, were purchased from Sigma Chemical Co. (St. Louis, MO). Bradford reagent was obtained from Bio-Rad Laboratories (Mississauga, Ontario, Canada).

6.3. NTPDase assays

Enzyme activity was measured by the release of inorganic phosphate with the malachite green colorimetric assay.[49] Relative activity and resistance to hydrolysis were determined at 37 °C, in 1 mL of the following incubation medium: 8 mM $CaCl_2$, 5 mM tetramisole, 50 mM imidazole, and 50 mM Tris-base buffered at pH 7.5. The enzyme preparation (1.1 μg) a bovine spleen particulate fraction, isolated as previously described,[50] was added to the incubation medium and pre-incubated for 3 min. The reaction was started by adding the substrate, either 100 μM of ATP or its analogues **4b** or **5b**, and stopped 7 min later with 250 μL of the malachite green reagent. Controls were run in parallel by adding the enzyme after the malachite green reagent. Enzyme hydrolysis was expressed as units, that is, μmol of P_i released/min/mg protein.[50] Protein concentration was estimated by the Bradford microplate assay, using bovine serum albumin as a reference standard.[51] All experiments were performed in triplicate.

6.4. Potato-apyrase assay

Enzyme activity was measured by the release of inorganic phosphorous as described above. The assay was performed at 37 °C in 1 mL of the following incubation medium: 8 mM $CaCl_2$, 50 mM Tris-base, 50 mM imidazole, buffered at pH 7.6. Resistance to hydrolysis was measured at 50 μM of either ATP or its analogues. In all cases, the reaction was started by the addition of 5.5×10^{-3} μg enzyme and stopped after 7 min with 250 μL of the malachite green reagent. The absorbance at 630 nm was measured 21 min after the reagent addition. Apparent K_m and V_{max} values for ATP and for each analogue were measured with substrate concentrations ranging between 12 and 200 μM and calculated from the experimental data by the Lineweaver–Burk plot of the analogues' hydrolysis. All experiments were performed in two replicates each in duplicate, and the results are expressed as the mean ± SEM.

The values for K_m and V_{max} with apyrase for ATP are: 36.8 ± 2.34 and 769.2 ± 0.015 and for **5b**: 44.72 ± 3.95 and 304.15 ± 1.41, respectively. Inhibition of ATP-hydrolysis by potato apyrase in the presence of 0.37 mM analogues **3b** and **4b** was measured and expressed in hydrolysis percentages: 75.0 ± 10.08 and 66.7 ± 9.1, respectively.

Acknowledgements

This work was supported in part by BMBF-MOS Grant No. 1812, and the Marcus Center for Medicinal Chemistry. A.R.B. and S.A.L. were supported by NSERC of Canada. The authors thank Mrs. Rachel Levi-Drumer and Prof. Benjamin Ehrenberg for helpful discussions.

References and notes

1. Warshel, A. *Biochemistry* **1981**, *20*, 3167.
2. Garcia-Moreno, B. E.; Dwyer, J. J.; Gittis, A. G.; Lattman, E. E.; Spencer, D. S.; Stites, W. E. *Biophys. Chem.* **1997**, *64*, 211–224, and references cited therein.
3. Kesvatera, T.; Jonsson, B.; Thulin, E.; Linse, S. *J. Mol. Biol.* **1996**, *259*, 828–839.
4. *Methods in Enzymology*; Rubin, B., Dennis, E. A., Eds.; Academic: NY, 1997; Vol. 284, part A, pp 138–139.
5. (a) Salahuddin, A.; Siddiqui, F. A.; Salahuddin, P. *Indian J. Biochem.* **1996**, *33*, 292–297; (b) Paradies, H. H.; Vettermann, W. *Arch. Biochem. Biophys.* **1979**, *194*, 88–100; (c) Voordouw, G.; Gaucher, G. M.; Roche, R. S. *Can. J. Biochem.* **1974**, *52*, 981–990.
6. (a) Johnson, C. S.; Vogtmann, L.; Deal, W. C., Jr. *Biochem. Biophys. Res. Commun.* **1976**, *73*, 391–395; (b) Lapanje, S.; Dolecek, V.; Kawahara, K.; Higashi, K. *Biophys. Chem.* **1974**, *2*, 369–376; (c) Trujillo, J. L.; Deal, W. C., Jr. *Biochemistry* **1977**, *16*, 3098–3104.
7. (a) Fischer, B.; Yefidoff, R.; Major, D. T.; Rutman-Halili, I.; Shneyvays, V.; Zinman, T.; Jacobson, K. A.; Shainberg, A. *J. Med. Chem.* **1999**, *42*, 2685–2696; (b) Fischer, B.; Chulkin, A.; Boyer, J. L.; Harden, T. K.; Gendron, F.-P.; Beaudoin, A. R.; Chapal, J.; Hillaire-Buys, D.; Petit, P. *J. Med. Chem.* **1999**, *42*, 3636–3646; (c) Halbfinger, J. L.; Major, D. T.; Ritzmann, M.; Ubl, J.; Reiser, G.; Boyer, J. L.; Harden, T. K.; Fischer, B. *J. Med. Chem.* **1999**, *42*, 5325–5337; (d) Major, D. T.; Halbfinger, E.; Fischer, B. *J. Med. Chem.* **1999**, *42*, 5338–5347; (e) Gendron, F.-P.; Halbfinger, E.; Fischer, B.; Duval, M.; D'Orleans-Juste, P.; Beaudoin, A. R. *J. Med. Chem.* **2000**, *43*, 2239–2247; (f) Zundorf, G.; Schafer, R.; Vohringer, C.; Halbfinger, E.; Fischer, B.; Reiser, G. *Biochem. Pharmacol.* **2001**, *61*, 1259–1269; (g) Major, D. T.; Laxer, A.; Fischer, B. *J. Org. Chem.* **2002**, *67*, 790–802.
8. (a) Kochetkov, N. K.; Shibaev, V. N.; Kost, A. A. *Tetrahedron Lett.* **1971**, *22*, 1993–1996; (b) Secrist, J. A., III. Barrio, J. R.; Leonard, N. J.; Weber, G. *Biochemistry* **1972**, *11*, 3499–3506; Thomas, R. W.; Leonard, N. J. *Heterocycles* **1976**, *5*, 839–882; (c) Leonard, N. J. *CRC Crit. Rev. Biochem.* **1984**, *15*, 125; (d) Leonard, N. J. *Biochem. Mol. Biol.* **1992**, *3*, 273–297.
9. Fischer, B.; Kabha, E.; Gendron, F.-P.; Beaudoin, A. R. *Nucleos. Nucleot.* **2000**, *19*, 1033–1054.
10. Callis, P. R. *Ann. Rev. Phys. Chem.* **1983**, *34*, 329–357.
11. (a) Kornblum, N.; Powers, J. W.; Anderson, G. J.; Jones, W. J.; Larson, H. O.; Levand, O.; Weaver, W. M. *J. Am. Chem. Soc.* **1957**, *79*, 6562; (b) Kornblum, N.; Jones, W. J.; Anderson, G. J. *J. Am. Chem. Soc.* **1959**, *81*, 4113–4114.
12. Torssell, K. *Acta Chem. Scand.* **1967**, *21*, 1–14.
13. Biernat, J.; Ciesiolka, J.; Gornicki, P.; Adamiak, R. W.; Krzyzosiak, W. J.; Wiewiorowski, M. *Nucleic Acids Res.* **1978**, *5*, 789–804.
14. *Org. Synth.* **1973**, *Vol. 5*, 552–554.
15. Vöhringer, C.; Schäfer, R.; Reiser, G. *Biochem. Pharmacol.* **2000**, *59*, 791–800.
16. Zündorf, G.; Schäfer, R.; Vöhringer, C.; Halbfinger, E.; Fischer, B.; Reiser, G. *Biochem. Pharmacol.* **2001**, *61*, 1259–1269.
17. (a) Traverso-Cori, A.; Chaimovich, H.; Cori, O. *Arch. Biochem. Biophys.* **1965**, *109*, 173–184; (b) Loss of less than 10% activity after two weeks at 4 °C. Personal observation.
18. Nakayama, H.; Yamaga, T. *Biophys. Chem.* **1998**, *75*, 1–6.
19. Spencer, R. D.; Weber, G.; Tolman, G. L.; Barrio, J. R.; Leonard, N. J. *Eur. J. Biochem.* **1974**, *45*, 425–429.
20. (a) Kochetkov, N. K.; Shibaev, V. N.; Kost, A. A. *Tetrahedron Lett.* **1971**, *22*, 1993–1996; (b) Secrist, J. A., III. Barrio, J. R.; Leonard, N. J.; Weber, G. *Biochemistry* **1972**, *11*, 3499–3506; (c) Thomas, R. W.; Leonard, N. J. *Heterocycles* **1976**, *5*, 839–882; (d) Leonard, N. J. *CRC Crit. Rev. Biochem.* **1984**, *15*, 125; (e) Leonard, N. J. *Biochem. Mol. Biol.* **1992**, *3*, 273–297.
21. Leonard, N. J.; Cruickshank, K. A. *J. Org. Chem.* **1985**, *50*, 2480–2488.
22. Wang, A. H. J.; Dammann, L. G.; Barrio, J. R.; Paul, I. C. *J. Am. Chem. Soc.* **1974**, *96*, 1205–1213.
23. Penzer, G. R. *Eur. J. Biochem.* **1973**, *34*, 297–305.
24. (a) Boarder, M. R.; Hourani, S. M. O. *Trends Pharmacol. Sci.* **1998**, *19*, 99–107; (b) Barnard, E. A.; Simon, J.; Webb, T. E. *Mol. Neurobiol.* **1997**, *15*, 103–129; (c) Inoue, K. *Pharmacol. Res.* **1998**, *38*, 323–331; (d) Chan, C. M.; Unwin, R. J.; Burnstock, G. *Exp. Nephrol.* **1998**, *6*, 200–207; (e) Burnstock, G. *J. Theor. Biol.* **1976**, *62*, 491–503.
25. (a) Bhagwat, S. S.; Williams, M. *Eur. J. Med. Chem.* **1997**, *32*, 183–193; (b) King, B. F.; Townsend-Nicholson, A.; Burnstock, G. *Trends Pharmacol. Sci.* **1998**, *19*, 506–514; (c) Abbracchio, M. P.; Burnstock, G. *Pharmacol. Therap.* **1994**, *64*, 445–475.
26. (a) Halbfinger, E.; Major, D. T.; Ritzmann, M.; Ubl, J.; Reiser, G.; Boyer, J. L.; Harden, T. K.; Fischer, B. *J. Med. Chem.* **1999**, *42*, 5325–5337; (b) Major, D. T.; Halbfinger, E.; Fischer, B. *J. Med. Chem.* **1999**, *42*, 5338–5347.

27. (a) van Rhee, A. M.; Fischer, B.; van Galen, P. J. M.; Jacobson, K. A. *Drug Des. Discov.* **1995**, *13*, 133–154; (b) Jiang, Q.; Guo, D.; Lee, B. X.; van Rhee, A. M.; Kim, Y. C.; Nicholas, R. A.; Schachter, J. B.; Harden, T. K.; Jacobson, K. A. *Mol. Pharmacol.* **1997**, *52*, 499–507; (c) Moro, S.; Guo, D.; Camaioni, E.; Boyer, J. L.; Harden, T. K.; Jacobson, K. A. *J. Med. Chem.* **1998**, *41*, 1456–1466; (d) Hoffmann, C.; Moro, S.; Nicholas, R. A.; Harden, T. K.; Jacobson, K. A. *J. Biol. Chem.* **1999**, *274*, 14639–14647; (e) Kim, H. O.; Barak, D.; Harden, T. K.; Boyer, J. L.; Jacobson, K. A. *J. Med. Chem.* **2001**, *44*, 3092–3108.
28. (a) Major, D. T.; Fischer, B. *J. Med. Chem.* **2004**, *47*, 4391–4404; (b) Major, D. T.; Nahum, V.; Wang, Y.; Reiser, G.; Fischer, B. *J. Med. Chem.* **2004**, *47*, 4405–4416.
29. Enjyoji, K.; Sévigny, J.; Lin, Y.; Frenette, P. S.; Christie, P. D.; Esch, J. S., II. Imai, M.; Edelberg, J. M.; Rayburn, H.; Lech, M.; Beeler, D. L.; Csizmadia, E.; Wagner, D. D.; Robson, S. C.; Rosenberg, R. D. *Nat. Med.* **1999**, *5*, 1010–1017.
30. Koziak, K.; Kaczmarek, E.; Kittel, A.; Seyigny, J.; Blusztajn, J. K.; Schulte Am Esch, J., II.; Imai, M.; Guckelberger, O.; Goepfert, C.; Qawi, I.; Robson, S. C. *J. Biol. Chem.* **2000**, *275*, 2057–2062.
31. (a) Lebel, D.; Poirier, G. G.; Phaneuf, S.; St Jean, P.; Laliberte, J. F.; Beaudoin, A. R. *J. Biol. Chem.* **1980**, *255*, 1227–1233; (b) Laliberte, J. F.; St-Jean, P.; Beaudoin, A. R. *J. Biol. Chem.* **1982**, *257*, 3869–3874.
32. Valenzuela, M. A.; Del Campo, G.; Marin, E.; Traverso-Cori, A. *Biochem. J.* **1973**, *133*, 755–763.
33. Shulte am Esch, J., II.; Sévigny, J.; Kaczmarek, E.; Siegel, J. B.; Imai, M.; Zoziak, K.; Beaudoin, A. R.; Robson, S. C. *Biochemistry* **1999**, *38*, 2248–2258.
34. (a) Scheller, K. H.; Hofstetter, F.; Mitchell, P. R.; Prijs, B.; Sigel, H. *J. Am. Chem. Soc.* **1981**, *103*, 247–260; (b) Scheller, K. H.; Sigel, H. *J. Am. Chem. Soc.* **1983**, *105*, 5891–5900; (c) Tribolet, R.; Sigel, H. E. *J. Biochem.* **1988**, *170*, 617–626.
35. (a) Hohne, W. E.; Heitmann, P. *Anal. Biochem.* **1975**, *69*, 607–617; (b) Vanderkooi, J. M.; Weiss, C. J.; Woodrow, G., III. *Biophys. J.* **1978**, *24*, 266–267; (c) Vanderkooi, J. M.; Weiss, C. J.; Woodrow, G., III. *Biophys. J.* **1979**, *25*, 263–275.
36. Rose, G. D.; Wolfenden, R. *Annu. Chem. Rev. Biophys. Biomol. Struct.* **1993**, *22*, 381–415.
37. (a) Gilson, M. K.; Honing, B. *Biopolymers* **1986**, *25*, 2097–2119; (b) Rupley, J.; Careri, G. *Adv. Protein Chem.* **1991**, *41*, 37–172; (c) Tredgold, R. H.; Hole, P. H. *Biochim. Biophys. Acta* **1976**, *443*, 137–142.
38. Sharp, K. A.; Honig, B. *Annu. Rev. Biophys. Biophys. Chem.* **1990**, *19*, 301–332.
39. Lakowicz, J. R. *Principles of Fluorescence Spectroscopy*, 2nd ed.; Kluwer Academic/Plenum: New York, 1999.
40. Iwaki, T.; Torigoe, C.; Noji, M.; Nakanishi, M. *Biochemistry* **1993**, *32*, 7589–7592.
41. Kung, C. E.; Reed, J. K. *Biochemistry* **1986**, *25*, 6114–6121, and references cited therein.
42. (a) Kung, C. E.; Reed, J. K. *Biochemistry* **1989**, *28*, 6678–6686; (b) Cox, G. S.; Hauptman, P. J.; Turro, N. J. *Photochem. Photobiol.* **1984**, *39*, 597–601.
43. Ferreira, S. T.; Gratton, E. *J. Am. Chem. Soc.* **1994**, *116*, 5791–5795.
44. Kamlet, M. J.; Abboud, J.-L. M.; Abraham, M. H.; Taft, R. W. *J. Org. Chem.* **1983**, *48*, 2877–2887.
45. D'Aprano, A.; Fuoss, R. M. *J. Phys. Chem.* **1969**, *73*, 400–406.
46. Rapp, W.; Klingenberg, H. H.; Lessing, H. E. *Ber. Bunsen-Ges.* **1971**, *75*, 883–886.
47. Andrew, T. C.; Tsin Hugo, A. *Life Sci.* **1988**, *43*, 1379–1384.
48. Grynkiewicz, G.; Poenie, M.; Tien, R. Y. *J. Biol. Chem.* **1985**, *260*, 3440–3450.
49. Baykov, A. A.; Evtushenko, O. A.; Avaeva, S. M. *Anal. Biochem.* **1988**, *171*, 266–270.
50. Sevigny, J.; Levesque, F. P.; Grondin, G.; Beaudoin, A. R. *Biochim. Biophys. Acta* **1997**, *1334*, 73–88.
51. Bradford, M. M. *Anal. Biochem.* **1976**, *72*, 248–254.